Capillary trapping of supercritical CO_2 in porous media at the pore scale

T. Suekane, T. Izumi & K. Okada
Department of Mechanical Engineering,
The University of Tokushima, Japan

Abstract

Carbon dioxide capture and storage in geological formations is recognized as a promising method for decoupling fossil fuel use and carbon emissions. Carbon dioxide injected into geological formations is expected to be trapped by several mechanisms against buoyancy. In this paper, we focused on capillary rapping. Trapped bubbles in packed beds of glass beads were visualized by means of micro-focused X-ray CT at pore scale for supercritical CO_2 and water systems at reservoir condition and for nitrogen and water systems at laboratory room condition. When the diameter of glass beads is the same, distribution of volume of trapped bubbles is similar for each condition. At the pressure of 8.5MPa and the temperature of 45ºC, which corresponds to just above a critical point, the morphology of the interface between the supercritical CO_2 and water suggests that CO_2 is non-wetting to glass beads. Residual gas saturation increases with a decrease in a diameter of glass beads, because the capillary pressure is higher with respect to buoyancy. Residual gas saturation can be expressed as a function of the reverse Bond number for each condition. Distribution of trapped bubble volume is identical with each other for each condition at same diameter of glass beads. The large trapped bubbles contribute to the residual gas saturation.
Keywords: capillary trapping, residual gas saturation, supercritical CO_2, micro-focused X-ray CT, carbon dioxide capture and storage.

1 Introduction

The geological storage of anthropogenic greenhouse gases to mitigate climate change is recognized as a means to reduce emissions to the atmosphere and the

WIT Transactions on Engineering Sciences, Vol 70, © 2011 WIT Press
www.witpress.com, ISSN 1743-3533 (on-line)
doi:10.2495/MPF110261

related impacts as a result of continues use of fossil fuels. Deep saline aquifers and depleted oil and gas reservoirs are potential subsurface deposits for CO_2 [1].

In geological formations, because of hydrostatic pressure and a geothermal gradient, pressure and temperature increase with depth. The critical condition of CO_2 (304 K and 7.38 MPa) is reached at a depth of approximately 700 m, where CO_2 density increases rapidly. However, the specific gravity of supercritical CO_2 at the condition which corresponds to the depths of 1000-3000m is about 0.7. Therefore, buoyancy brings CO_2 upwards. On the other hand, four trapping mechanisms have been identified [1]: structural trapping, capillary trapping, solubility trapping and mineralization trapping. CO_2 injected into the geological formations is expected to be stored by these trapping mechanisms for long time. During a storage period, each trapping mechanism changes relative weight increasing security and stability of storage [2–4].

The mechanism of capillary trapping can be explained as follows from the pore-scale point of view. CO_2 is injected into geological formation by replacing saline water forming a large continuous plume. After the CO_2 injection has stopped, saline water imbibes back into the formation. During this imbibition process, a continuous CO_2 plume is disconnected to form CO_2 bubbles of which volume is in the order of the pore of porous rock. At the pore-scale capillary pressure acting on a CO_2 bubble is expected to be greater than buoyancy and/or viscous force. As a result, CO_2 bubbles are eventually trapped in porous media. Capillary rapping has some advantages. Firstly, it plays an important role from the early stage of CO_2 storage. Secondly, it is capable of storing a large amount of CO_2 per unit volume of the formation [5].

As capillary trapping has been receiving growing attention, residual CO_2 saturation has been investigated experimentally in laboratory core-flooding experiments [5–9]. Because the capillary trapping takes place for a CO_2 bubble at pore-scale, microscopic approaches are taken to investigate its mechanism [10–13]. X-ray computed microtomography has provided a tool for the non-destructive investigation of the three-dimensional microstructure of porous media. Non-destructive direct imaging approaches are attractive because they provide not only a detailed and unique description of the pore-space geometry but also fluid flow within them [14–22]. The X-ray microtomography has been also applied to investigation of CO_2 trapping in porous media [5, 10, 12, 13].

The objective of this article is to study residual gas trapping in packed beds of glass beads at pore scale. A number of gas trapping experiments are conducted with supercritical CO_2 at elevated pressure and temperature and with nitrogen with room condition for various diameters of packing spheres. Characteristics of residual gas trapping of supercritical CO_2 are discussed comparing images obtained with nitrogen at the pore scale. The residual gas saturation has been analysed using the Bond number, which denotes the ratio of the buoyancy to the capillary pressure.

2 Experimental methodology and equipment

2.1 Dimensionless parameters and experimental conditions

A bubble of non-wetting phase in porous media is under the influence of capillary force, buoyancy and viscous pressure gradient. The ratios of gravity to capillary forces and viscous to capillary forces are expressed as dimensionless groups, known respectively as the Bond number, Bo, and capillary number Ca [23]:

$$\mathrm{Bo} = \frac{(\rho_w - \rho_n)gR^2}{\sigma} \tag{1}$$

$$\mathrm{Ca} = \frac{\mu_w u_w}{\sigma} \tag{2}$$

where, ρ is density, g is acceleration due to gravity, R is particle radius, σ is interfacial tension, μ is viscosity, u is displacing fluid velocity, and subscripts w and n denote wetting phase and non-wetting phase, respectively.

Experimental conditions are summarized in Table 1. Experiments of capillary trapping were carried out at two conditions. One is the condition of the pressure of 8.5 MPa and the temperature of 45ºC which corresponds to the depth of approximately 850 m. At this condition, CO_2 is in a supercritical state. The other is normal laboratory room condition where we used nitrogen as a non-wetting phase instead of CO_2 to reduce the dissolution in water. Interfacial tension between supercritical CO_2 and water is about half of that between nitrogen and water in laboratory room condition. Because of high density of supercritical CO_2 with respect to nitrogen, buoyancy also is lower for supercritical CO_2. As a result, the Bond number falls in similar range for glass beads radius of 50–300 μm.

Table 1: Experimental conditions [24–26].

		Viscosity	Density	Interfacial tension	Capillary number	Bond number
		μ [μPa·s]	ρ [kg/m^3]	σ [mN/m]	Ca [-]	Bo [-]
Reservoir condition (45ºC, 8.5MPa)	$scCO_2$	20	259.6	35.7	1.0×10^{-5} - 4.0×10^{-5}	5.0×10^{-4} - 1.8×10^{-2}
	H_2O	600	993.9			
Lab. room condition (20ºC, 0.1MPa)	N_2	17.87	1.123	72.6	1.0×10^{-6}	3.4×10^{-4} - 1.2×10^{-2}
	H_2O	1062	996.7			

2.2 Experimental setup and procedure

Residual gas trapping has been investigated at the microscopic level using a micro-focused X-ray CT scanner (Comscantechno Co. ScanXmate-RB090SS). The magnification ratio of X-ray CT scanners depends on the ratio of the

distance between the X-ray detector and the X-ray source, and that between an object and the X-ray source. When a packed bed with a low diameter is placed close to the X-ray source, highly magnified images can be achieved.

Two types of packed bed of glass beads were used for the experiments. One is designed to elevate temperature and pressure which correspond to the reservoir at the depth of about 850 m as shown in Fig. 1a. Glass beads were packed in a titanium tube with inner and outer diameter of 3 mm and 4 mm which could resist pressure up to 20 MPa. The packed bed made of titanium tube was placed in an acrylic resin pipe with outer diameter of 14 mm, where water was circulated to adjust temperature. The other is a simple packed bed used for the experiments at room temperature and pressure. Glass beads were packed in an acrylic resin tube with inner diameter of 10 mm at the height of about 40 mm.

The packed bed was vertically aligned in the X-ray CT scanner. The experimental set-up for high pressure and temperature experiments is shown in Fig. 1b. First, the structure of a backed bed was scanned at dry condition. Next, water was injected vertically upwards. At the same time, pressure was increased to be 8.5 MPa by an automatic back pressure regulator, while temperature was controlled to be 45ºC by water circulation. After water injection stopped, a syringe pump forced liquid CO_2 into piping at the flow rate of 1.0 ml/min. to establish the condition of irreducible water saturation. In piping, the CO_2 was heated to a supercritical state of 45ºC before arriving at the packed bed. Finally,

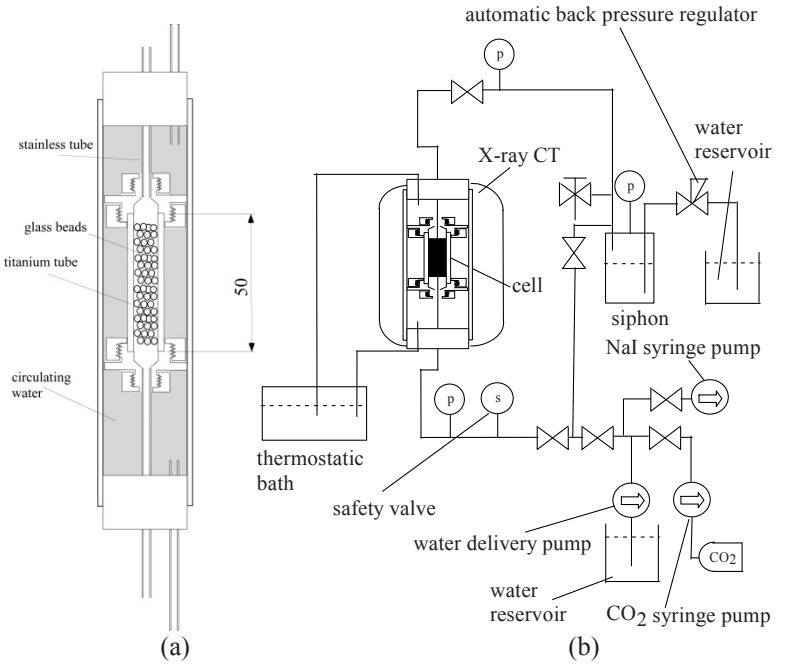

Figure 1: Pressure cell (a) and experimental setup (b) for elevated pressure and temperature.

water was injected into the packed bed at a constant flow rate which corresponds to the capillary number in the range between 1.0×10^{-5} and 4.0×10^{-5}. Water was saturated with CO_2 in advance in order to reduce dissolution of supercritical CO_2 in the packed bed. Between each process, the packed bed was scanned by X-ray CT.

In the case of a simple packed bed, experiments were carried out at laboratory room temperature and pressure. Nitrogen was used for a gas phase to prevent the dissolution of gas in water. Water was injected into the packed bed at the flow rate of 0.322 ml/min. which corresponds to the capillary number of 1.0×10^{-6}.

Water used in the experiments for both packed beds was doped with sodium iodide (NaI) at 7.5 wt% to enhance attenuation of X-ray. Reconstructed three-dimensional images consist of 608 × 608 × 610 pixels at a resolution of 12.66 μm/pixel and 24.91μm/pixel for experiments in reservoir condition and laboratory room condition, respectively, in all directions.

3 Results and discussion

Distribution of trapped bubbles in packed bed of glass beads with a diameter of 200 μm is shown in Fig. 2. The residual gas saturation was 16% and 20% for reservoir and laboratory room conditions, respectively. In the case of nitrogen at laboratory room condition, trapped gas bubbles distribute uniformly throughout the packed bed as shown in Fig. 2b. The size of trapped gas bubbles changes from a small bubble which locates at the centre of single pore to a large bubble which spreads over several pores. The interface between nitrogen and water suggests that nitrogen is perfectly non-wetting to glass beads. In the case of

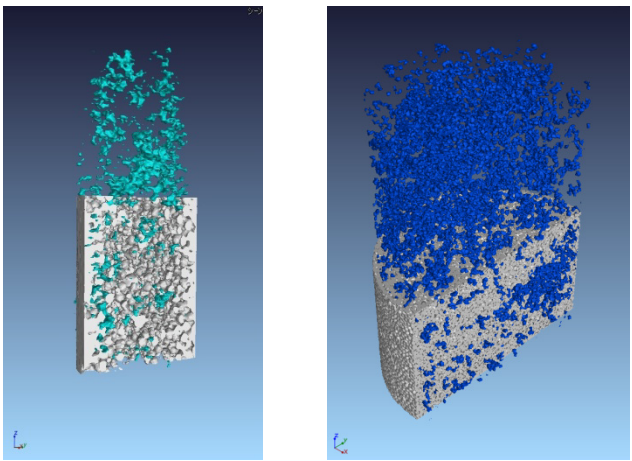

(a) (b)

Figure 2: Distribution of trapped gas bubbles in packed bed of glass beads with the diameter of 200 μm in reservoir condition (a) and laboratory room condition (b).

supercritical CO_2 at reservoir condition, the size of trapped bubbles changes also in the same range with the nitrogen case. The interface between supercritical CO_2 and water suggests that supercritical CO_2 is non-wetting to glass beads at this condition (45ºC, 8.5MPa) that is close to a critical point. Pentland *et al*. [9] has been reported that the contact angle of the interface between supercritical CO_2 and de-ionized water increases with a pressure increase up to 40 MPa. Figure 2a visualizes glass beads and CO_2 bubbles in a cylindrical region with the diameter of 3 mm inside of a titanium tube. In the region close to the outer edge, surfaces of glass beads are hard to recognize, because of artefacts caused by a titanium tube.

Based on the CT images, residual gas saturation, which is defined as volume ratio of trapped bubbles to pore, is evaluated for each experiment as shown in Fig. 3. With a decrease in the diameter of glass beads, residual gas saturation increases for both conditions, because capillary pressure tends to be higher compared to buoyancy. Even though the capillary number at laboratory room condition is about one order of magnitude lower than that at reservoir condition, residual saturation can be expressed with simple relationship with the inverse Bond number.

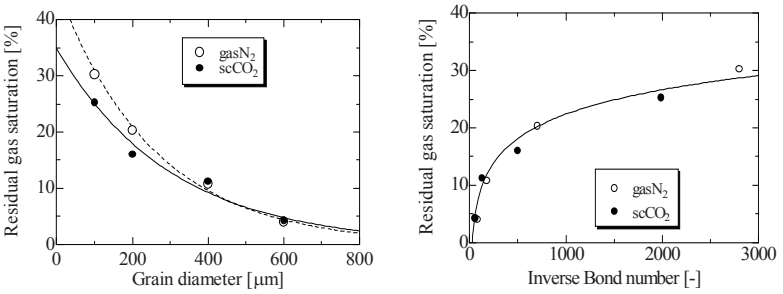

(a) (b)

Figure 3: Residual gas saturation vs. diameter of glass beads (a) and the inverse bond number (b) for reservoir and laboratory room conditions.

The volume of each trapped bubble was evaluated by three-dimensional image analysis software ImageJ [27, 28] with some plug-ins based on CT images such as shown in Fig. 2. The volume of trapped bubble is normalized with the volume of glass beads as shown in Fig. 4. In the packed bed of glass beads with the diameter of 600 μm, it is rare to find large trapped bubbles which spread over several pores for both conditions, because of buoyancy. Therefore, the residual gas saturation is lower for this packed bed. On the other hand, in the packed beds of fine glass beads the volume of some trapped bubbles is more than ten times higher than that of glass breads. As a result, the residual gas saturation is higher for these packed beds.

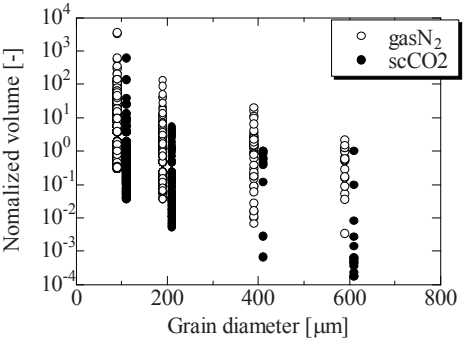

Figure 4: Distribution of the volume of trapped gas bubbles.

Contribution of gas bubbles in each volume range to residual gas saturation is shown in Fig. 5 for packed beds with various diameters of glass beads. The larger trapped bubbles contribute the more to the residual gas saturation for each condition and for each diameter of glass beads. With a decrease in the diameter of glass beads, much larger trapped bubbles contribute to the residual gas saturation for each condition.

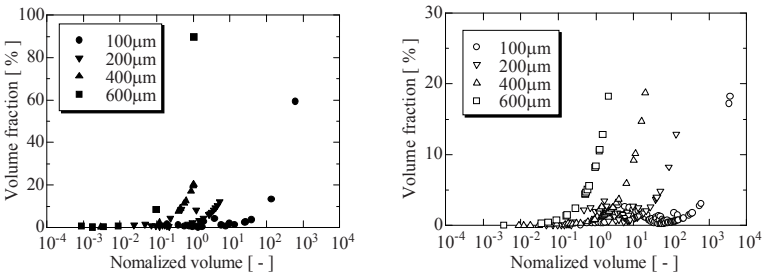

Figure 5: Contribution to residual gas saturation as a function of the volume of each bubble at reservoir condition (a) and laboratory room condition (b).

4 Conclusions

Trapped bubbles in packed beds of glass beads were visualized by means of micro-focused X-ray CT at pore scale for supercritical CO_2 and water systems at reservoir condition and for nitrogen and water systems at laboratory room condition. When the diameter of glass beads is same, distribution of volume of trapped bubbles is similar for each condition. At the pressure of 8.5MPa and the temperature of 45ºC, which corresponds to just above a critical point, the morphology of the interface between the supercritical CO_2 and water suggests

that CO_2 is non-wetting to glass beads. Residual gas saturation increases with a decrease in a diameter of glass beads, because the capillary pressure is higher with respect to buoyancy. Residual gas saturation can be expressed as a function of the reverse Bond number for each condition. Distribution of trapped bubble volume is identical with each other for each condition at same diameter of glass beads. The large trapped bubbles contribute to the residual gas saturation.

References

[1] Metz, B., Davidson, O., de Coninck, H.C., Loos, M. & Meyer, L.A. (eds.), *IPCC Special Report on Carbon Dioxide Capture and Storage*, Cambridge University Press, Cambridge, pp. 195-276 , 2005.

[2] Doughty, C., Investigation of CO_2 plume behavior for a large-scale pilot test of geologic carbon storage in a saline formation. *Trans. Porous Med.*, **82(1)**, pp.49-76, 2010.

[3] Juans, R., MacMinn, C.W. & Szulczewski, M.L., The footprint of the CO_2 plume during carbon dioxide storage in saline aquifer: storage efficiency for capillary trapping at the basin scale. *Trans.Porous Med.*, **82(1)**, pp. 19-30, 2010.

[4] Bachu, S., CO_2 storage in geological media: role, means, status and barriers to deployment. *Progress in Energy and Combustion Science*, **34**, pp. 254-273, 2008.

[5] Suekane, T., Nobuso, T. Hirai, S. & Kiyota, M., Geological storage of carbon dioxide by residual gas and solubility trapping. *Intern. J. Greenhouse Gas Control*, **2(1)**, pp. 58-64, 2008.

[6] Bennion, D.B. & Bachu, S., Dependence on temperature, pressure, and salinity of the IFT and relative permeability displacement characteristics of CO_2 injected in deep saline aquifers. Presented at the 2006 SPE Annual Technical Conference and Exhibition, San Antonio, Texas, USA, 24-27 September, SPE 102138, 2006.

[7] Iglauer, S., Carbon capture and storage with a focus on capillary trapping as a mechanism to store carbon dioxide in geological porous media (Chapter 4). *Advances in Multiphase Flow and Heat Transfer*, eds. L. Cheng and D. Mewes, 3, pp. 177-197, Bentham e Books [in press].

[8] Al Mansoori, S.K., Itsekiri, E., Iglauer, S., Pentland C.H., Bijeljic, B. & Blunt, M.J., Measurements of non-wetting phase trapping applied to carbon dioxide storage. *Intern. J. Greenhouse Gas Control*, **4**, pp. 283-288, 2010.

[9] Pentland C.H., El-Maghraby, R., Georgiadis, A., Iglauer, & Blunt, M.J., Immiscible displacement and capillary trapping in CO_2 storage. Presented at International Conference on Greenhouse Gas Control Technologies (GHGT-10), Amsterdam, Netherland, 2010.

[10] Zhou, N., Matsumoto, T., Hosokawa, T. & Suekane, T., Pore-scale visualization of gas trapping in porous media by X-ray CT scanning. *Flow Measurement and Instrumentation*, **21**, pp. 262-267, 2010.

[11] Suekane, T., Zhou, N., Hosokawa, T. & Matsumoto, T., Direct observation of gas bubbles trapped in sandy porous media. *Transport in Porous Media*, 82**(1)**, pp. 111-122, 2010.
[12] Wildenschild, D., Armstrong R.T., Herring, A.L., Young, I.M. & Carey, J.W., Exploring capillary trapping efficiency as a function of interfacial tension, viscosity, and flow rate. Presented at International Conference on Greenhouse Gas Control Technologies (GHGT-10), Amsterdam, Netherland, 2010.
[13] Ott, H., de Kloe, K., Marcelis, F. & Makurat, A., Injection of supercritical CO_2 in brain saturated sandstone: pattern formation during salt precipitation. Presented at International Conference on Greenhouse Gas Control Technologies (GHGT-10), Amsterdam, Netherland, 2010.
[14] Prodanović, M., Lindquist, W.B. & Seright, R.S., 3D image-based characterization of fluid displacement in a Berea core. *Advanced in Water Resources*, **30**, pp. 214-226, 2007.
[15] Al-Raoush, R.I. & Willson, C.S., A pore-scale investigation of a multiphase porous media system, *J. Contaminant Hydrology*, **77**, pp. 67-89, 2005.
[16] Bakke, S., & Øren, P.E., 3-D pore-scale modeling of sandstones and flow simulations in the pore networks, *SPEJ*, **2**, pp. 136-149, 1997.
[17] Prodanović, M., Lindquist, W.B. & Seright, R.S., Residual fluid blobs and contact angle measurements from X-ray images of fluid displacement. *Presented at the Computational Methods in Water Resources XVI Conference,* Copenhagen, Denmark, June 19-22, 2006.
[18] Wildenschild, D., Hopmans, J.W., Vaz, C.M.P., Rivers, M.L., Rikard, D. & Christensen, B.S.B., Using X-ray computed tomography in hydrology: systems, resolutions, and limitations. *J. Hydrology*, **267**, pp. 285-297, 2002.
[19] Al-Raoush, R.I. & Willson, C.S., Extraction of physically realistic pore network properties form three-dimensional synchrotron X-ray microtomography images of unconsolidated porous media systems. *J. Hydrology*, **300**, pp. 44-64, 2005.
[20] Øren, P.E. & Bakke, S., Process based reconstruction of sandstones and prediction of transport properties. *Transport in Porous Media*, **46**, pp. 311-343, 2002.
[21] Knackstedt, M.A., Sheppard, A.P. & Sahimi, M., Pore network modelling of two-phase flow in porous rock: the effect of correlated heterogeneity. *Advanced in Water Resources*, **24**, pp. 257-277, 2001.
[22] Soltani, A., Le Ravalec-Dupin, M. Fourar, M. & Rosenberg, E., Three-dimensional characteristics of permeability at the core scale. *Transport in Porous Media*, **84**, pp. 285-305, 2010.
[23] Morrow, N.R. & Songkran, B., Effect of viscous and buoyancy forces on nonwetting phase trapping in porous media. *Surface Phenomena in Enhanced Oil Recovery*, ed. Shah, D.O., Plenum Press, New York, pp. 387-411, 1981.
[24] Hebach, A., Oberhof, A., Dahmen, N., Kögel, A., Ederer, H. & Dinjus, E., Interfacial tension at elevated pressures-measurements and correlations in

the water + carbon dioxide system. *J. Chem. Data*, **47**, pp. 1540-1546, 2002.
[25] Bachu, S. & Bennion, D.B., Dependence of CO_2-brine interfacial tension on aquifer pressure, temperature and water salinity. *Energy Procedia*, 1, pp. 3157-3164, 2009.
[26] JSME, JSME Data Book: Thermophysical Properties of Fluids, Maruzen Co. Ltd., Tokyo, 1983.
[27] Abramoff, M. D., Magelhaes, P. J. & Ram, S. J., Image processing with imageJ. *Biophotonics Int.,* **11**, pp.36-44, 2004.
[28] Rasband, W. S., 1997-2008. ImageJ [Internet]. Bethesda (Maryland, USA): US National Institute of Health. Available from: http://rsbweb.nih.gov/ij/.